SUPPORTING INFORMATION

Terpyridine-based ruthenium complexes containing 4,5-diazafluoren-9-one ligand with light-driven enhancement of biological activity

Francisca Mayara Santos de Alencar,[a] Florencio Sousa Gouveia Jr,[a] Geângela de Fátima Sousa de Oliveira,[a] Alexandre Lopes Andrade,[b] Mayron Alves de Vasconcelos,[c] Alejandro Pedro Ayala,[d] Ana Claudia Silva Gondim,[a] Idalina Maria Moreira de Carvalho, [a] Carlos André Ferreira Moraes,[e] Marcos Vinícius Palmeira de Mello, [e] Alzir Azevedo Batista, [e] Luiz Gonzaga de França Lopes,[a*] Eduardo Henrique Silva Sousa[a*]

a- Group of Bioinorganic, Department of Organic and Inorganic Chemistry, Federal University of Ceara, Fortaleza, Brazil

b- Integrated Biomolecular Laboratory, Department of Pathology and Legal Medicine, Federal University of Ceara, Fortaleza, Brazil

c - Faculty of Education of Itapipoca, State University of Ceara (UECE), Itapipoca Brazil.

d- Department of Physics, Federal University of Ceara, Fortaleza, Brazil

e - Department of Chemistry, Federal University of São Carlos, Fortaleza, Brazil

*Corresponding authors: eduardohss@dqoi.ufc.br; lopeslu@dqoi.ufc.br

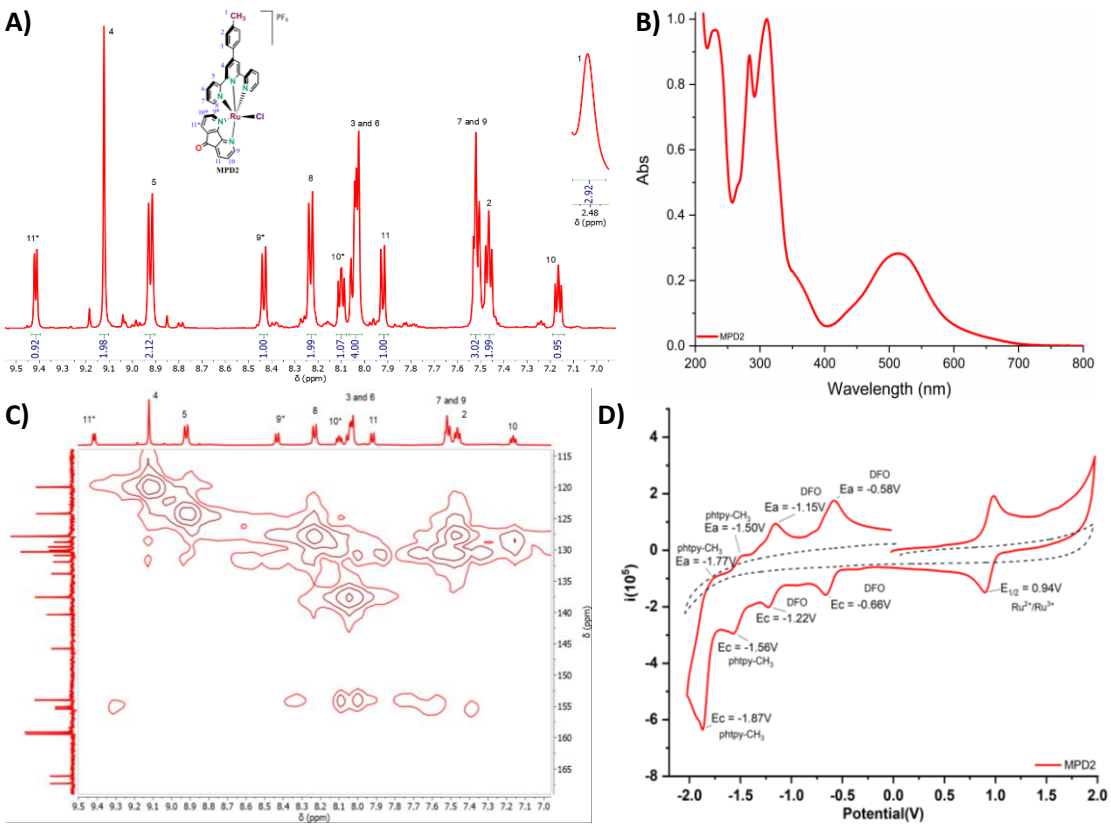

Fig. S1. For the **MPD2** complex: A) ^{1}H NMR in $(CD_3)_2SO$; B) Electronic absorption spectra in acetonitrile (3 x 10^{-5} mol L^{-1}) at 25 ºC; C) HSQC in $(CD_3)_2SO$; D) Cyclic voltammogram in 0.1 mol L^{-1} $TBAPF_6$/acetonitrile at 25 °C, at a scan rate of 0.100 Vs^{-1}, using glassy carbon, platinum wire and Ag|AgCl as working, auxiliary and reference electrodes, respectively (ferrocene redox pair used as 0.0 V reference). The black dashed line represents a swept potential for the electrolyte solution only.

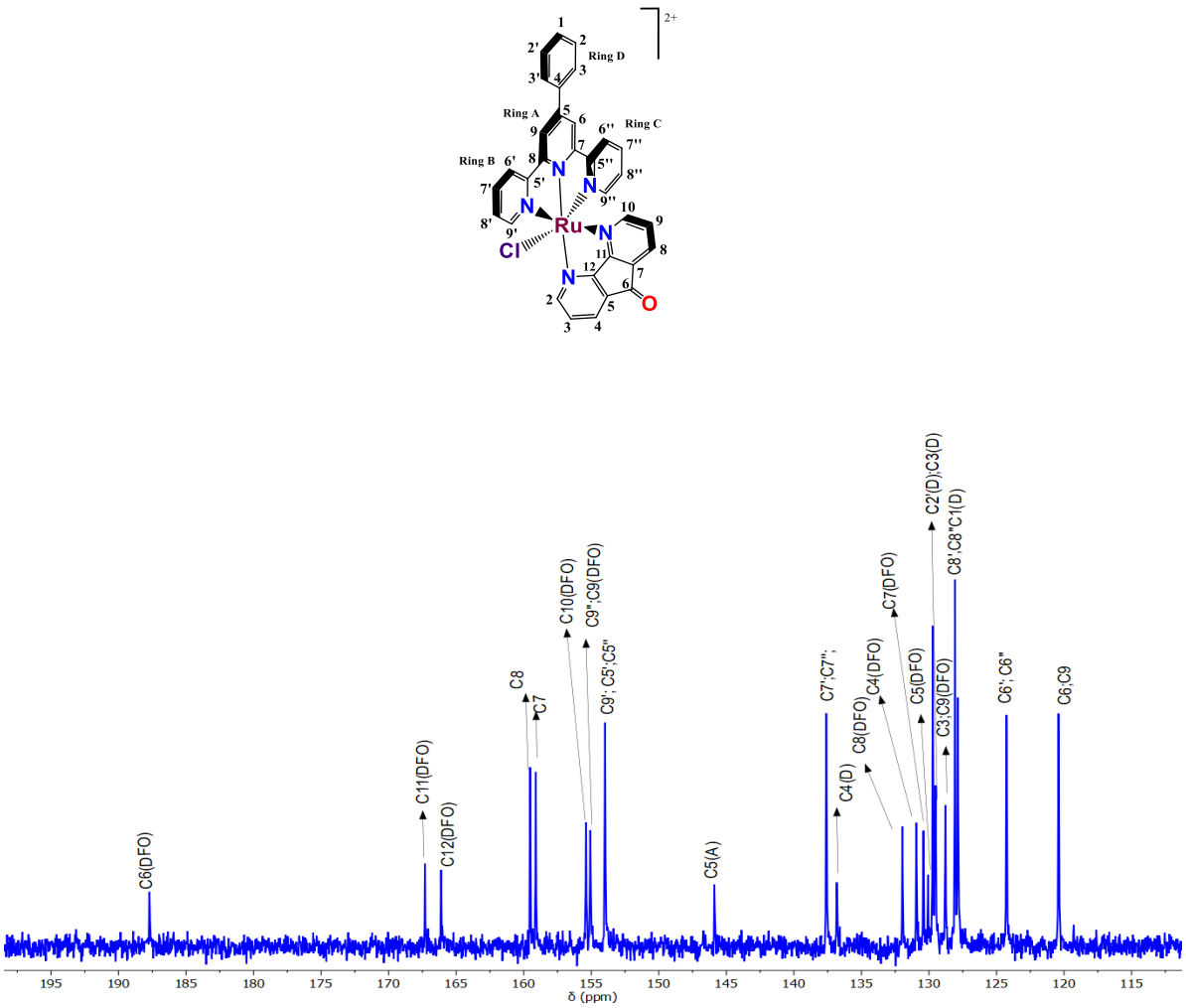

(A)

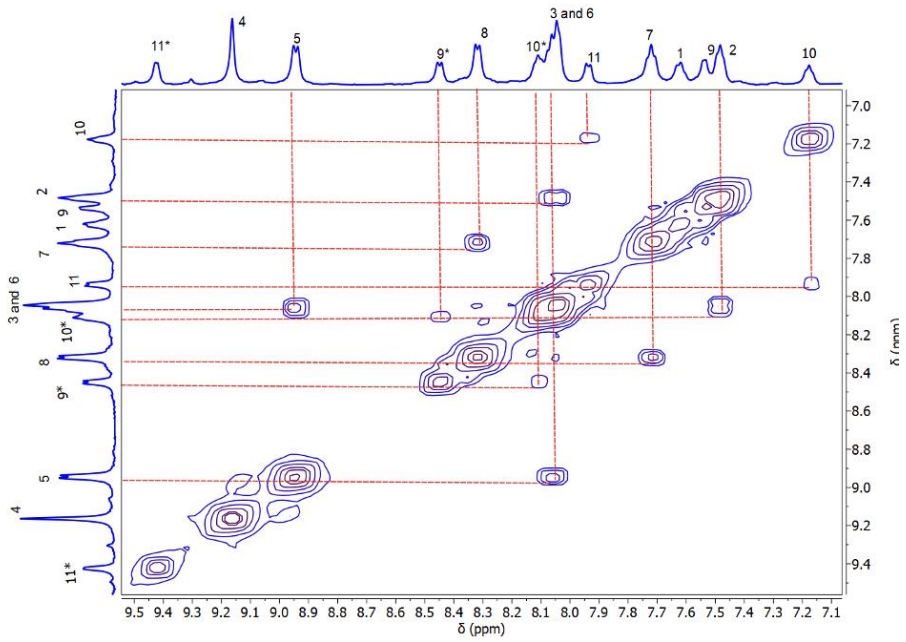

(B)

Fig. S2. ^{13}C NMR for **MPD1 (A)** and COSY **(B)** in $(CD_3)_2SO$.

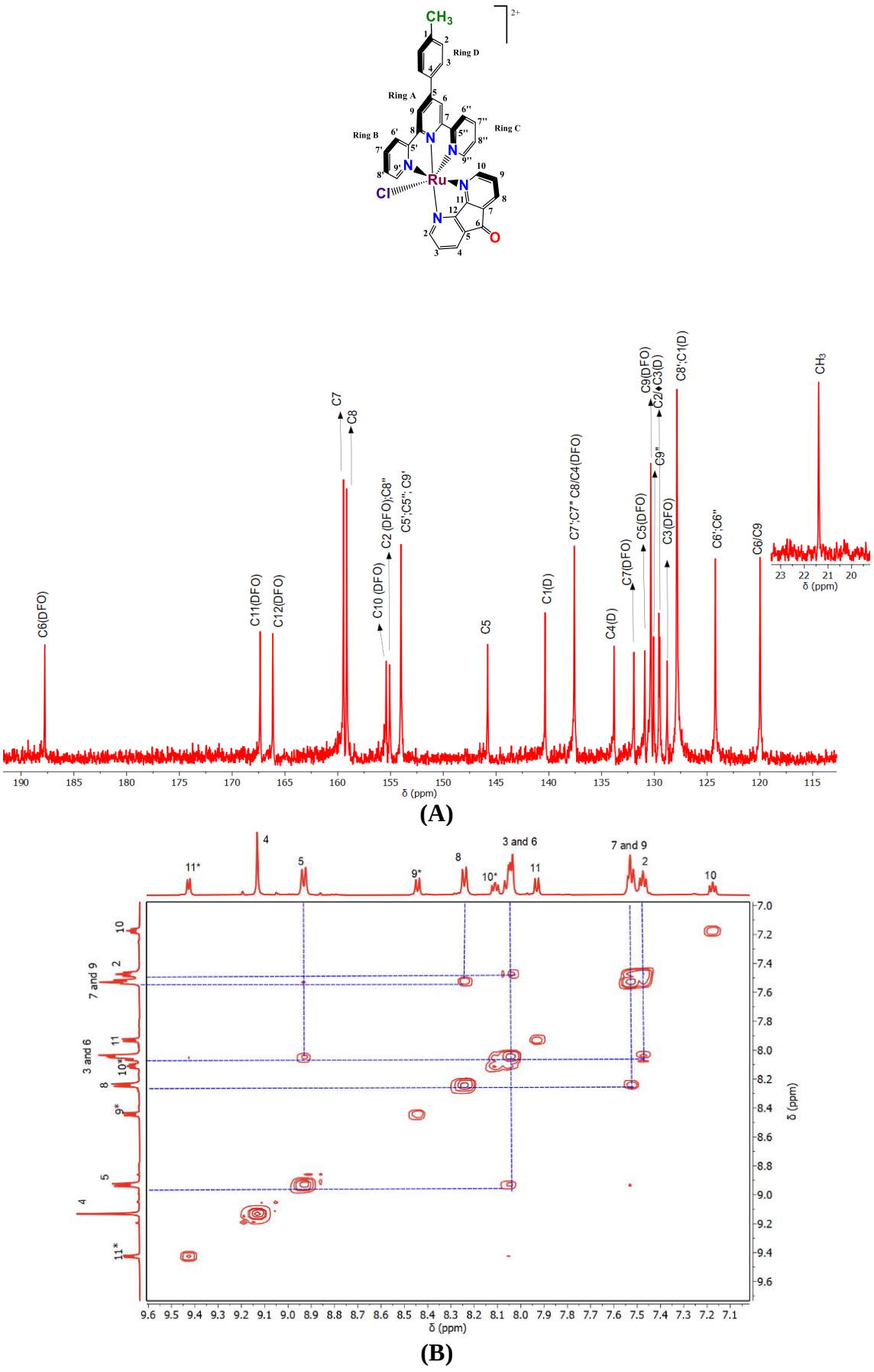

Fig. S3. ^{13}C NMR for **MPD2 (A)** and COSY **(B)** in $(CD_3)_2SO$.

(A)

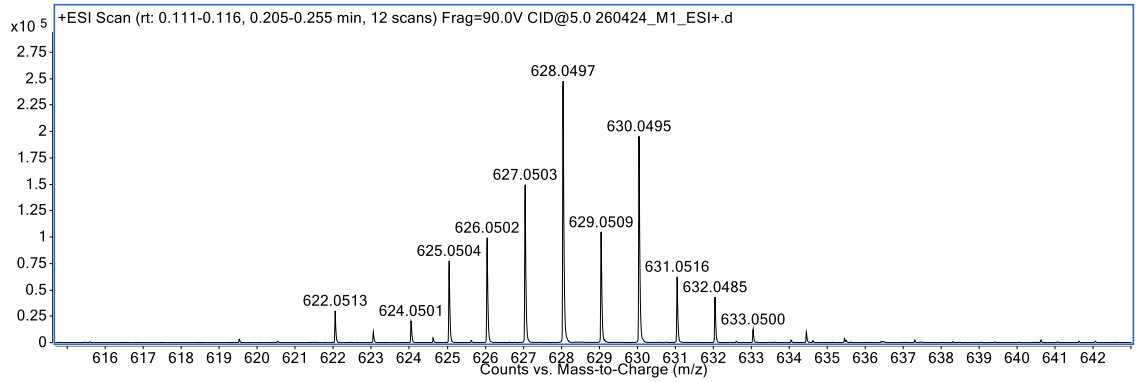

(B)

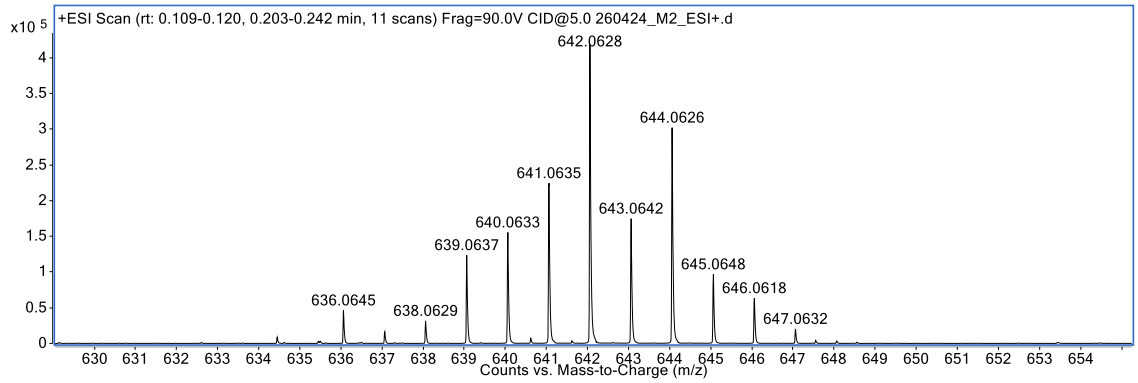

Fig. S4. High resolution mass spectrometry (ESI-TOF) for **MPD1** (A) and **MPD2** (B) in acetonitrile.

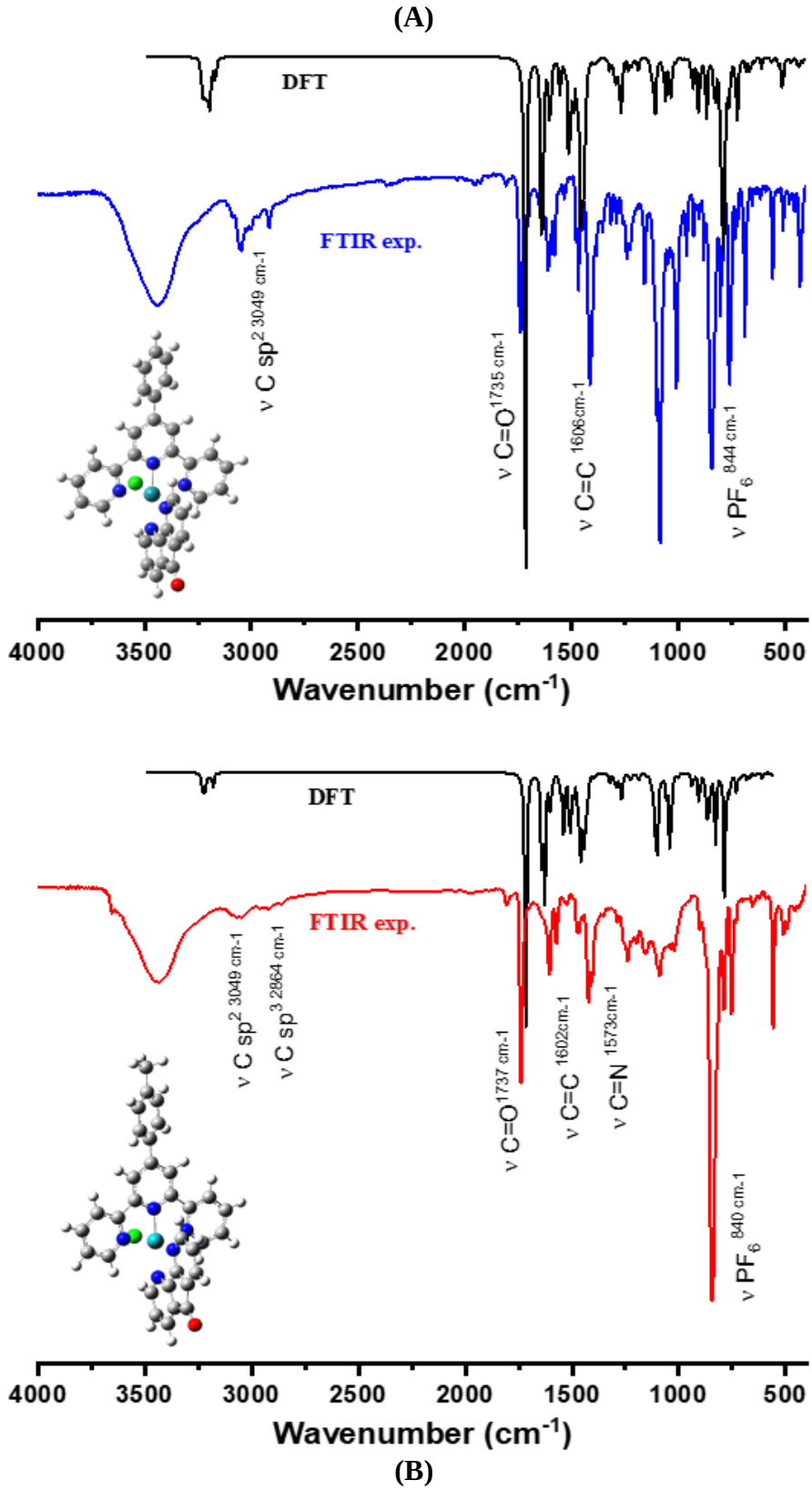

Fig. S5. Experimental FTIR spectra of (A) MPD1 and (B) MPD2 complexes dispersed in KBr (red lines) and calculated IR spectrum ions complexes (black lines). Inset: shows optimized structures of **MPD1** and **MPD2** in vacuum.

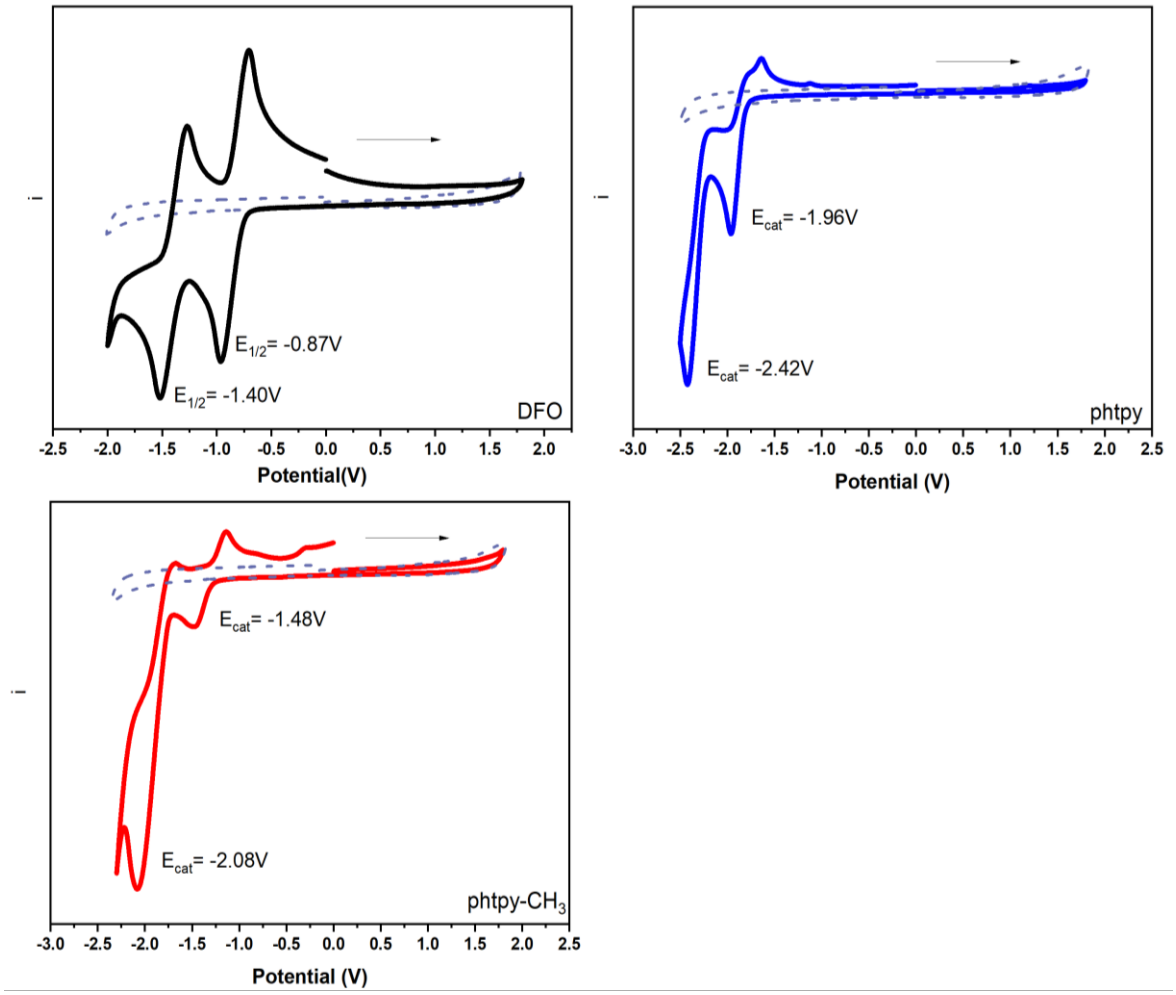

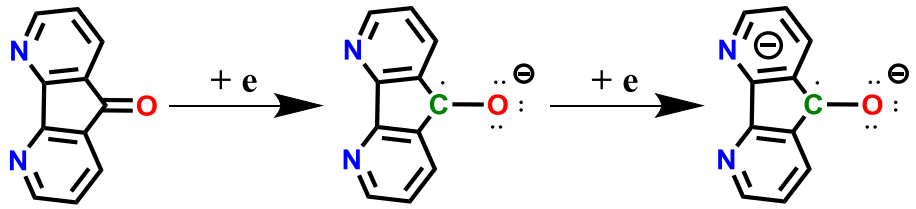

Fig. S6. Cyclic voltammograms of DFO (top, left), phtpy (top, right) and CH_3-phpty ligands (middle, left) carried out in 0.1 mol L^{-1} $TBAPF_6$ electrolyte in acetonitrile, at a scan rate of 0.100 Vs^{-1}, using glassy carbon, platinum wire and Ag|AgCl as working, auxiliary and reference electrodes, respectively (ferrocene redox pair used as 0.0 V reference); black dashed line represents the electrochemical scan of only the 0.1 mol L^{-1} $TBAPF_6$ electrolyte in acetonitrile, and DFO ligand reduction scheme (bottom).

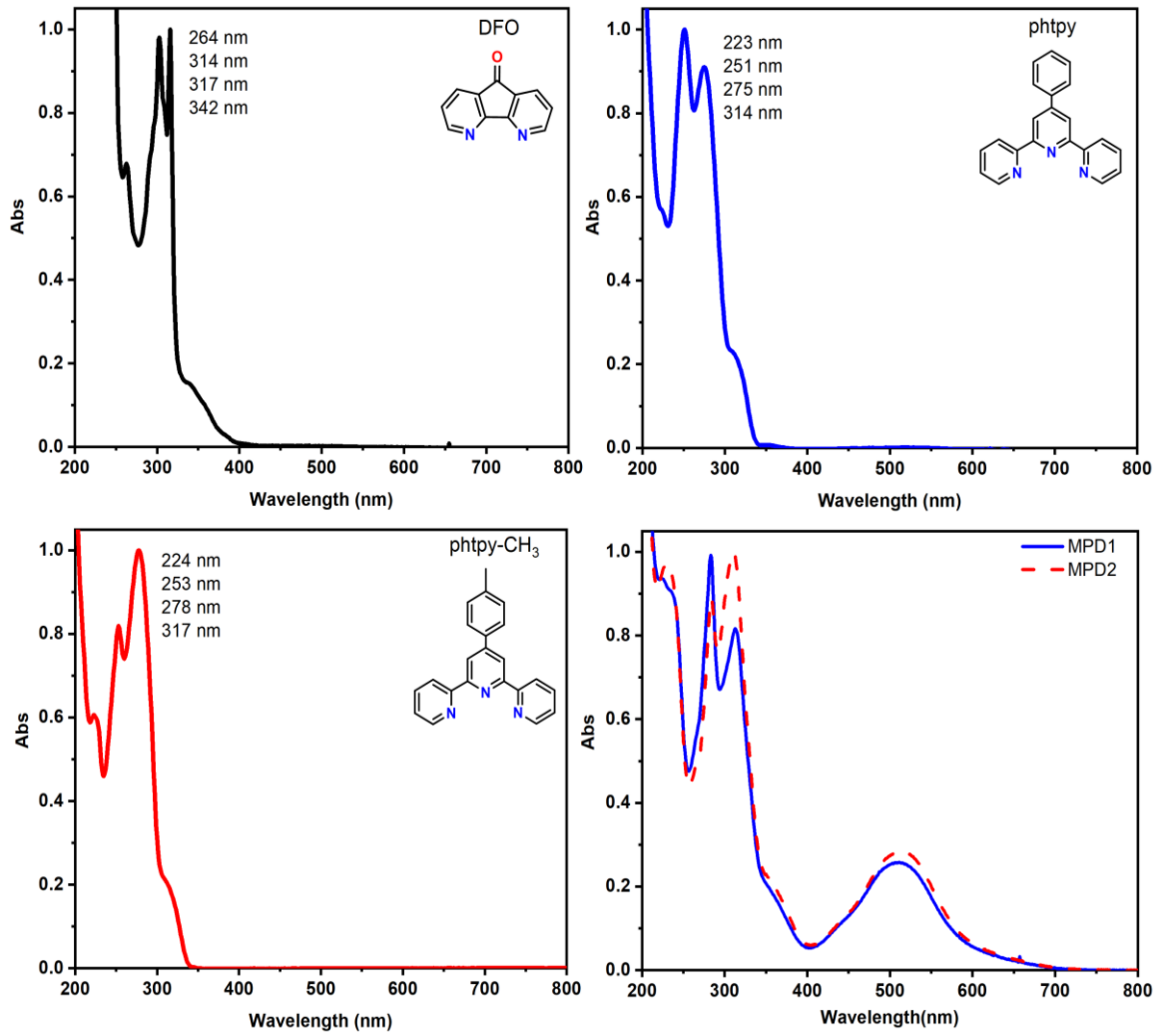

Fig. S7. Electronic absorption spectra of **DFO** (top, left), **phtpy** (top, right), **phtpy-CH$_3$** (bottom, left), **MPD1** and **MPD2** (3 x 10^{-5} mol L^{-1}, bottom right), in acetonitrile at 25 ^{o}C.

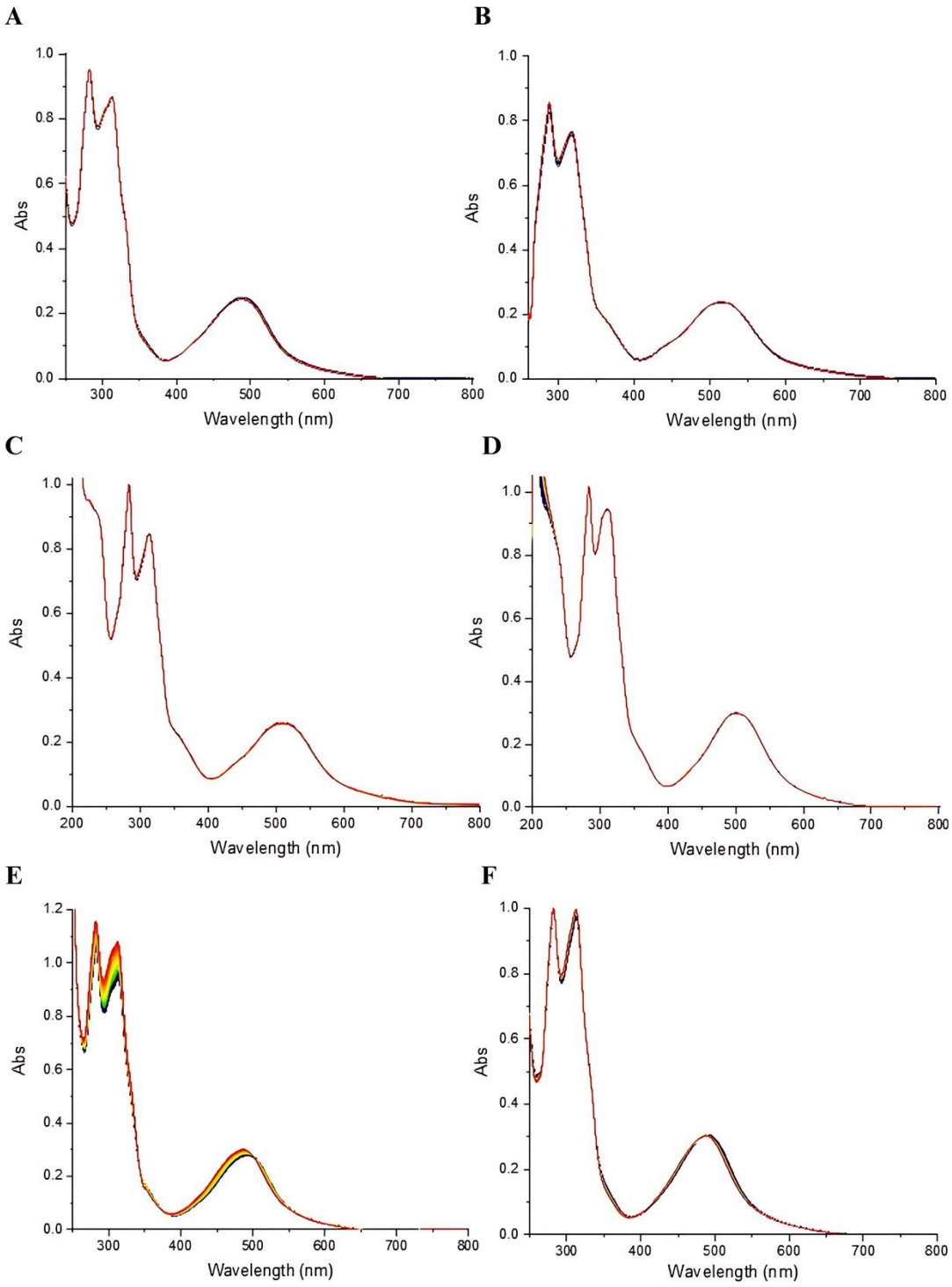

Fig. S8. Monitoring stability of **MPD1** (3×10^{-5} mol L^{-1}) under the following conditions: in 0.1 mmol L^{-1} phosphate buffer pH 7.4 (A), DMSO (B), acetonitrile (C) and methanol (D) in the dark for 2 h; or in 0.1 mmol L^{-1} phosphate buffer pH 7.4 (E) monitored for 24 h and in 0.1 mmol L^{-1} phosphate buffer pH 7.4 (F) irradiated with blue light for 2 h at 25 ^{o}C.

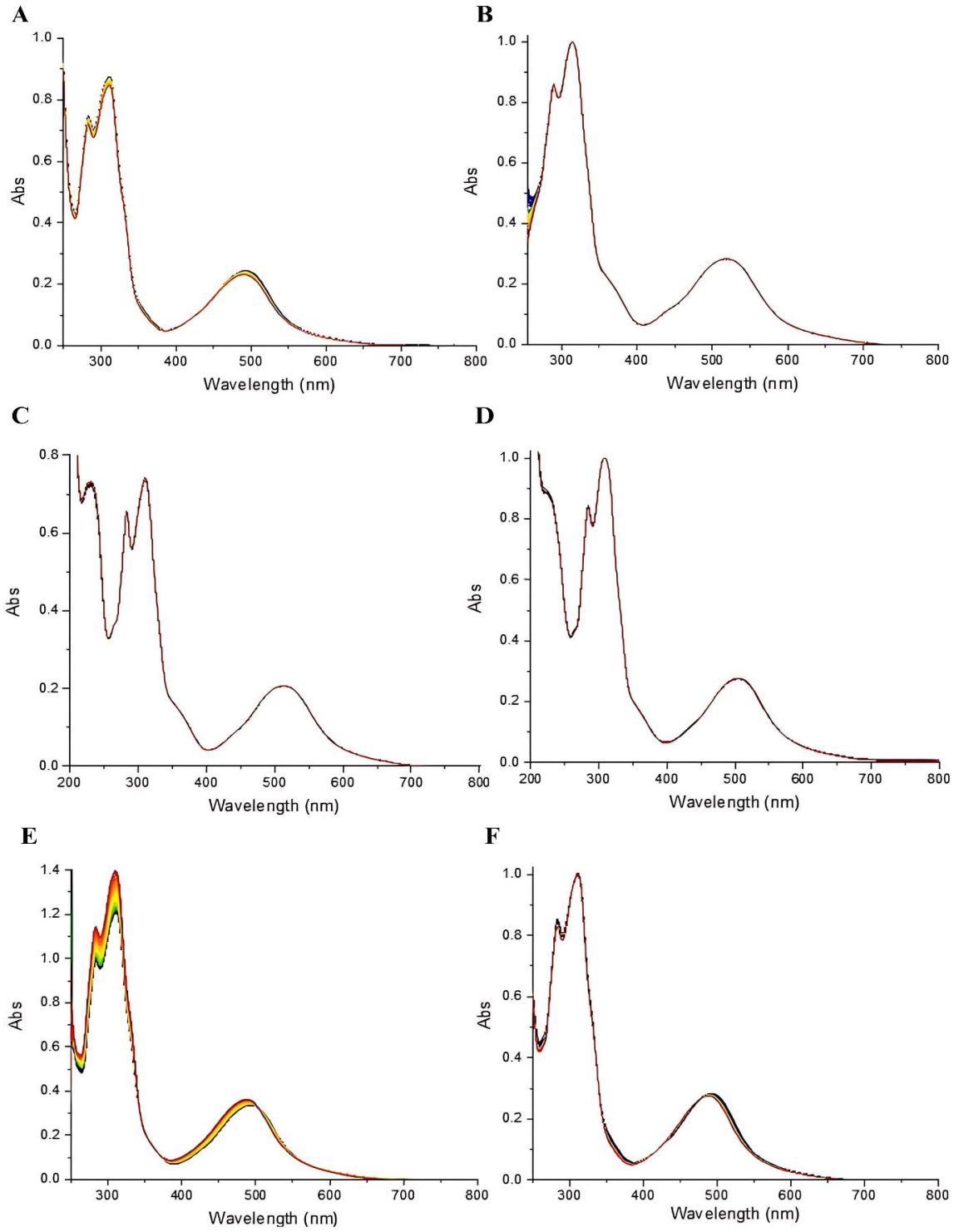

Fig. S9. Monitoring stability of **MPD2** (3×10^{-5} mol L^{-1}) under the following conditions: in 0.1 mmol L^{-1} phosphate buffer pH 7.4 (A), DMSO (B), acetonitrile (C) and methanol (D) in the dark for 2 h; or in 0.1 mmol L^{-1} phosphate buffer pH 7.4 (E) monitored for 24 h and in 0.1 mmol L^{-1} phosphate buffer pH 7.4 (F) irradiated with blue light for 2 h at 25 ^{o}C.

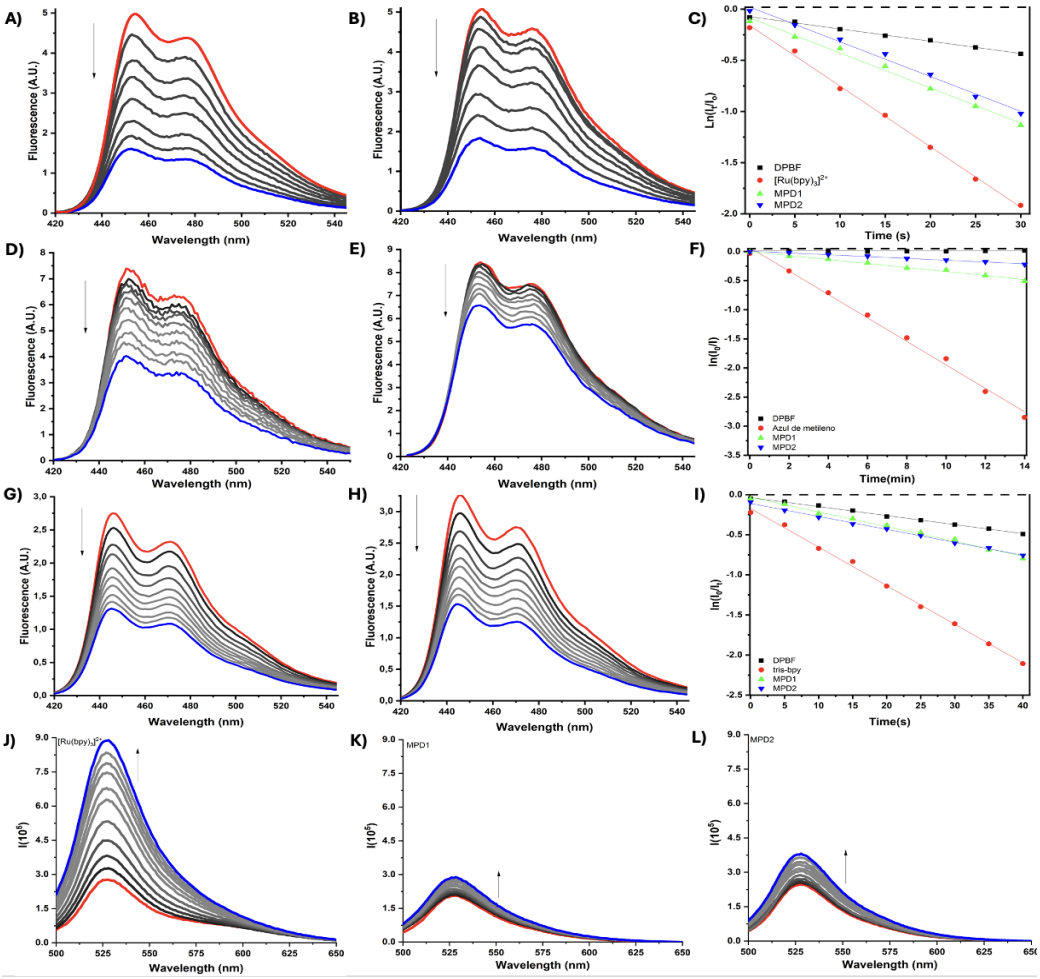

Fig. S10. Production of reactive oxygen species as singlet oxygen using DPBF and SOSG. Panel A and B show the emission spectra of DPBF 10 μmol L^{-1} with **MPD1** and **MPD2** 10 μmol L^{-1} upon blue light irradiation, respectively, in acetonitrile. Panels D and E show emission spectra of similar sample upon red light irradiation. Panels G and H show emission spectra of similar sample upon blue light irradiation in methanol. Panels C and I show time-dependent curves for relative emission for quantum yield measurements of samples irradiated with blue light in acetonitrile or methanol, respectively, while panel F shows these measurements irradiated with red light in acetonitrile. The black squares are of DPBF only, red triangles of **MPD1**, green diamond of **MPD2** and blue circles of the standard probe ($[Ru(bpy)_3]^{2+}$). Panels J, K and L show the emission spectra of SOSG 5 μmol L^{-1} with **MPD1** and **MPD2** 10 μmol L^{-1} upon blue light irradiation, respectively, in methanol.

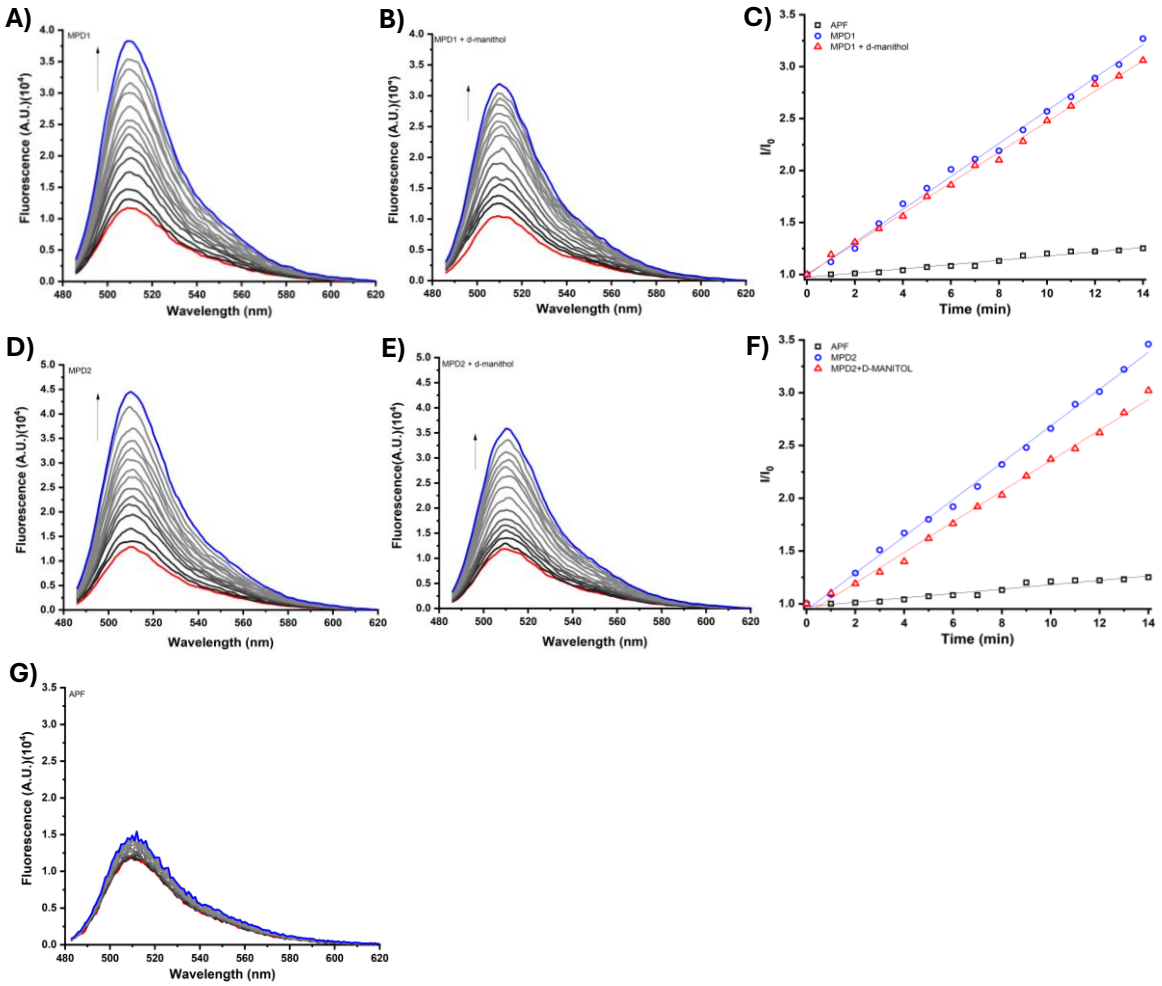

Fig. S11. Production of reactive oxygen species as hydroxyl radical using APF. Panels A and D show the emission spectra of **MPD1** and **MPD2** 10 μmol L^{-1} with APF 5 μmol L^{-1} upon blue light irradiation in 0.1 mmol L^{-1} tris buffer pH 7.4, respectively; Panels B and E show emission spectra of **MPD1** and **MPD2** with d-mannitol upon blue light irradiation. Panels C and F shows time-dependent curves for relative emission for quantum yield measurements of hydroxyl radicals, irradiated with blue light, where black squares are of APF only, blue circles are of the metal complexes and red triangles are of the metal complexes+d-mannitol. Panel G shows the emission spectra for a sample of only APF irradiated with blue light.

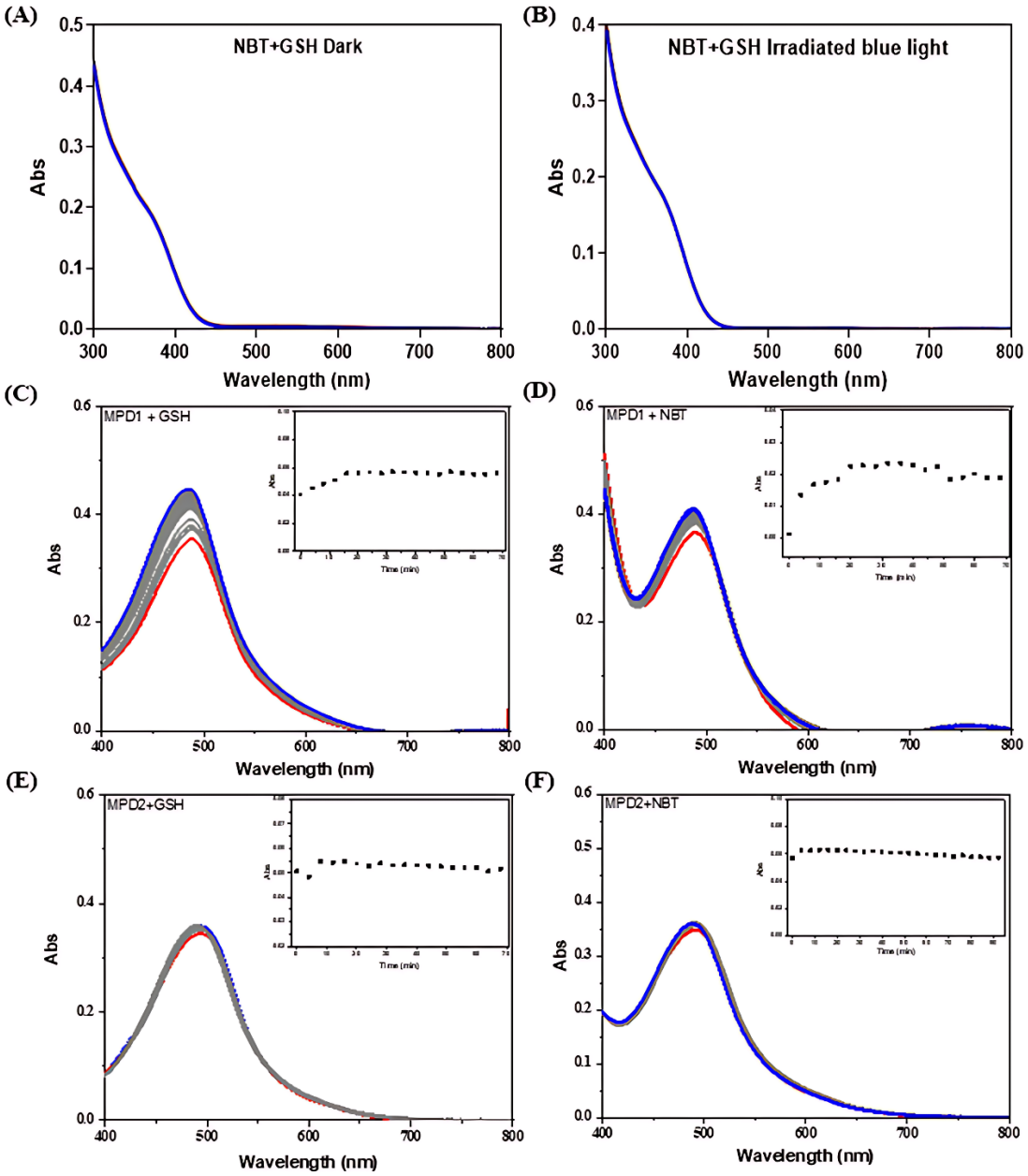

Fig. S12. Monitoring the mixture of MPD1 and MPD2 35 μmol L^{-1}; NBT 50 μmol L^{-1} and glutathione 1.5 mmol L^{-1} in 0.1 mol L^{-1} phosphate buffer pH 7.4, for 1 h under the following conditions: A) in the dark; B) irradiated with blue light. Other reaction controls involving the mixture of the metal complexes with NBT or GSH: C) GSH and MPD1 only irradiated with blue light; D) NBT and MPD1 only irradiated with blue light; E) GSH and MPD2 only irradiated with blue light; F) NBT and MPD2 only irradiated with blue light.

(A) **(B)**

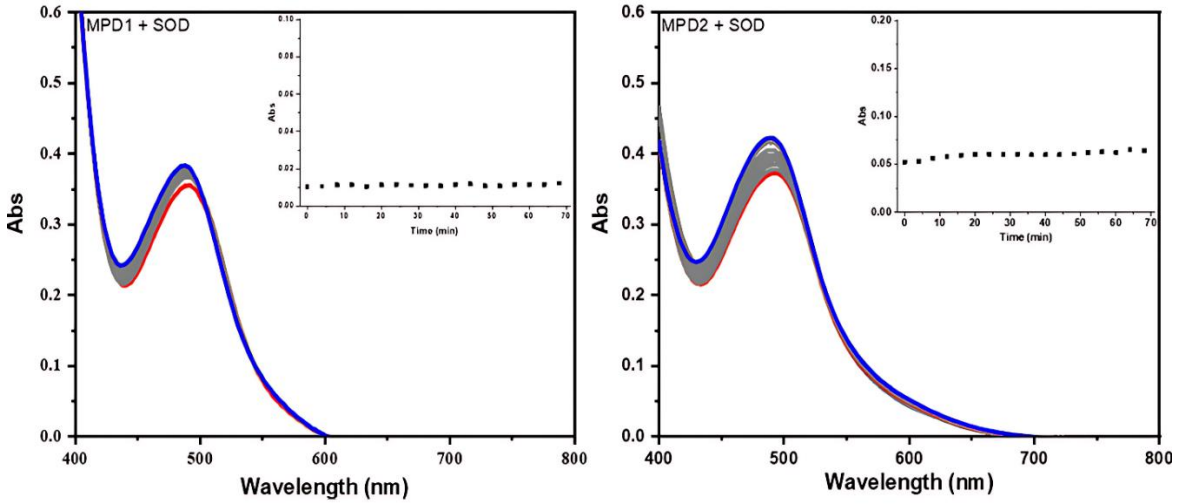

(C)

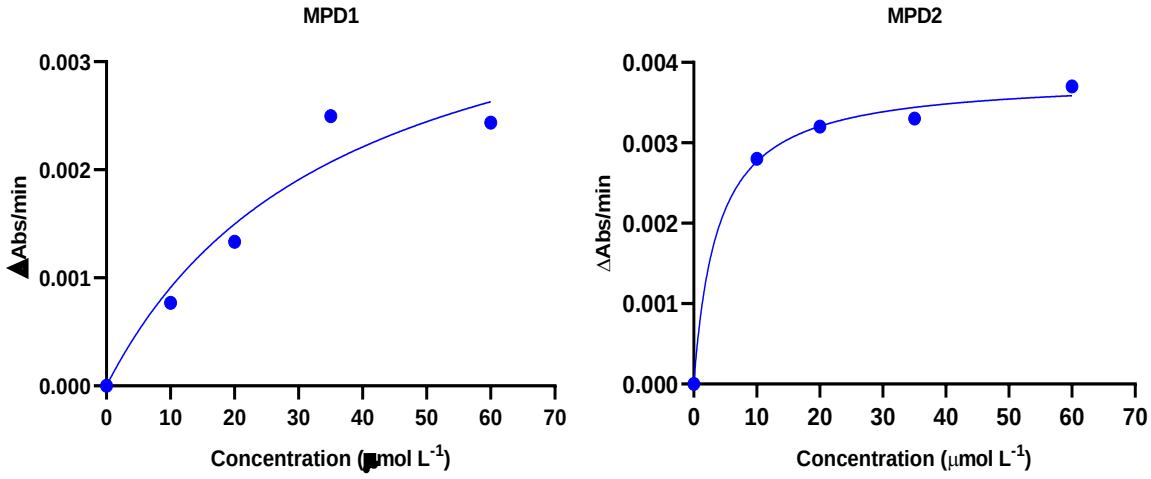

Fig. S13. Detection of the superoxide radical by the complexes **MPD1** and **MPD2** (35 µmol L^{-1}), in 0.1 mol L^{-1} phosphate buffer pH 7.4, GSH 1.5 mmol L^{-1}, NBT 50 µmol L^{-1}, SOD 4.4 U/mL, under the following conditions: a) **MPD1**, irradiated with blue light, with GSH, NBT and SOD; b) **MPD2**, irradiated with blue light, with GSH, NBT and SOD; c) Plot of the rate of superoxide radical production from the reaction of **MPD1** and **MPD2** complexes.

The stages of the cycle can be described as follows:

1. Production of superoxide by oxidation of Ru(II).

- Chemical equations:

$Ru(II) + O_2 \rightarrow O_2^{\bullet-}$

$Ru(III) + GSH \rightarrow Ru(II) + GS^{\bullet}$

$GS^{\bullet} + GS^{\bullet} \rightarrow GSSG$

2. Reduction of Ru(III) by GSH.

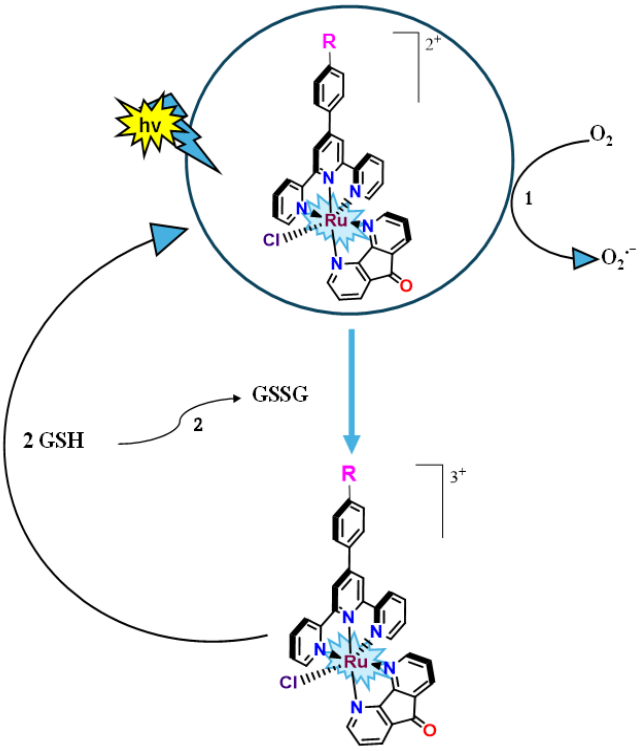

Fig. S14. Proposal of a catalytic cycle for the reduction of the metal complexes by GSH with the production of superoxide radical.

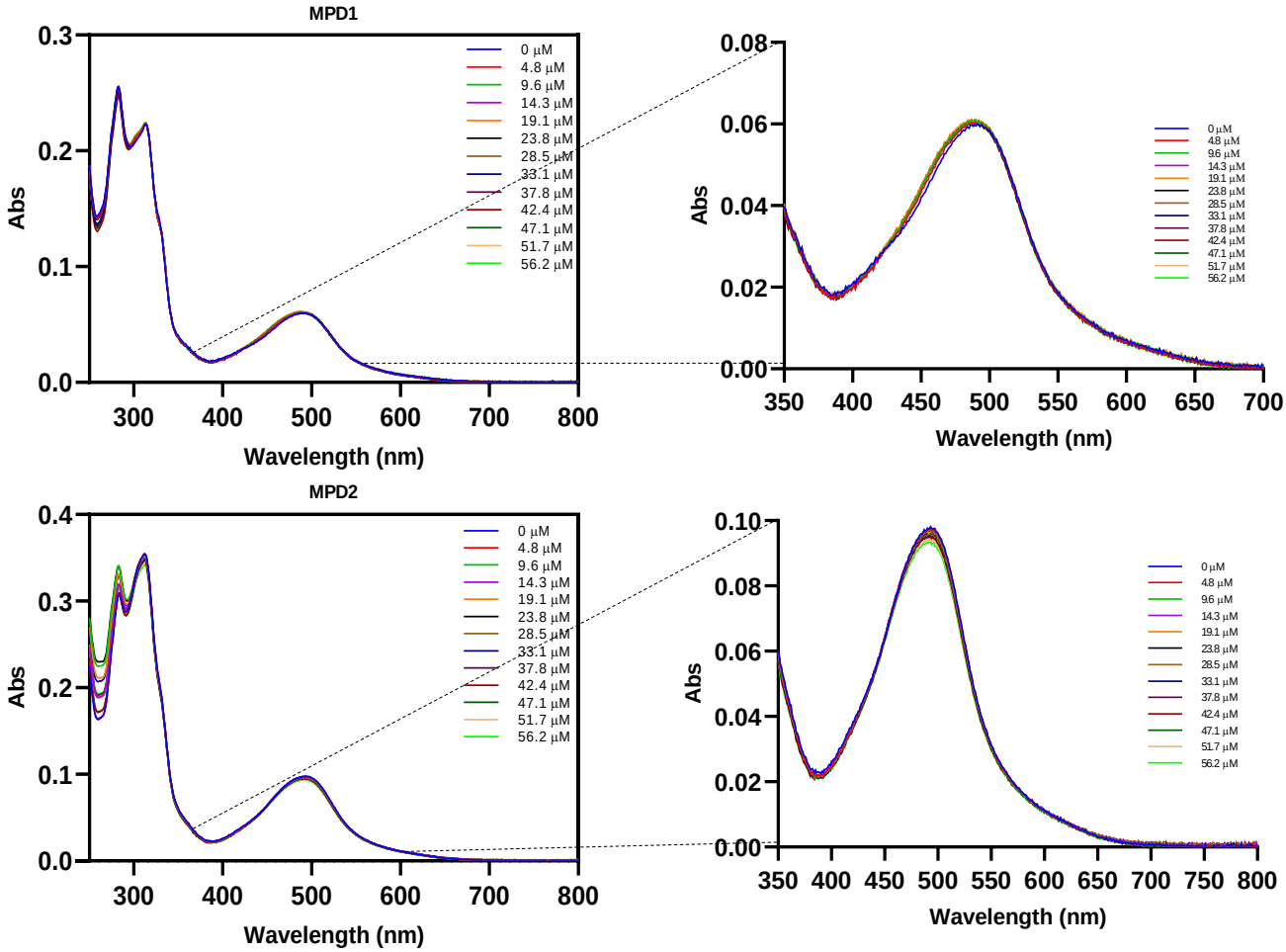

Fig. S15. DNA binding measurements. Panels show titration of **MPD1** (top) and **MPD2** (bottom) with calf thymus DNA monitored by UV-vis electronic spectroscopy, in 0.1 mmol L^{-1} tris-HCl pH 7.4 at 25 ºC.

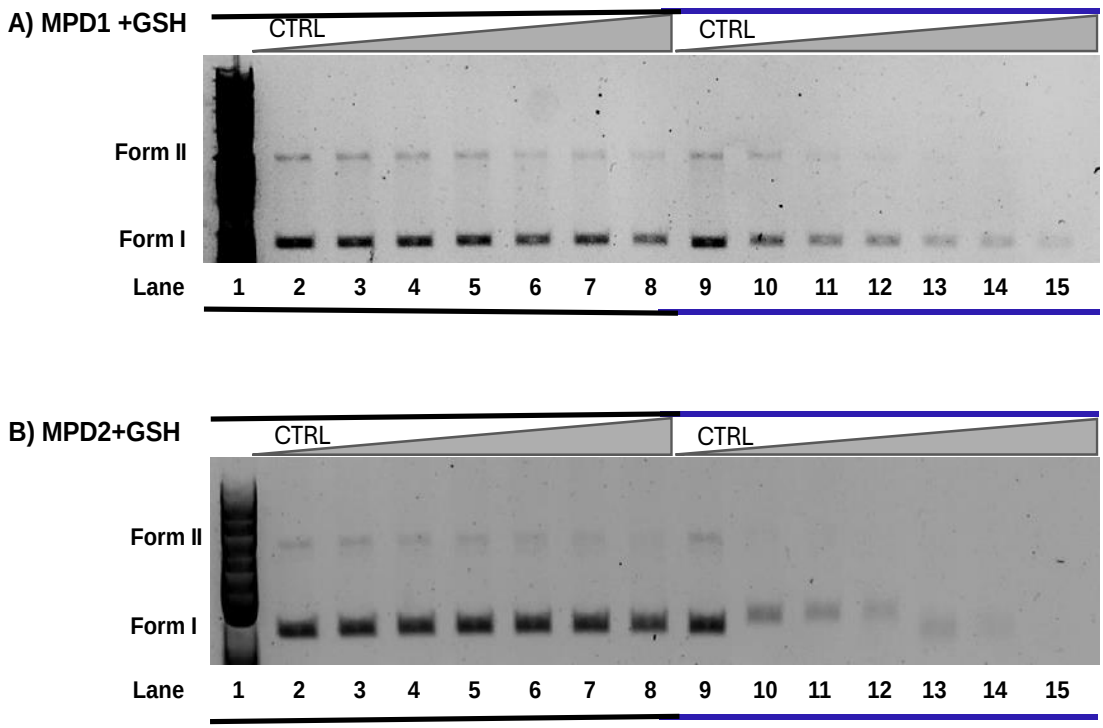

Fig. S16. Photocleavage of 20 μmol L^{-1} (in base pairs) of pUC19 DNA in the presence of **MPD1** or **MPD2** and GSH (5 mmol L^{-1}) either in the dark or upon 1 h of blue LED irradiation (negative images). In all experiments, lane 1 contains only linear DNA ladder, while lanes 2 and 9 contain only pUC19 DNA, and lanes 3-8 or 10-15 contained pUC19 with **MPD1** (Panel A) and **MPD2** (Panel B) at increasing concentrations (5, 10, 20, 30, 40 and 60 μmol L^{-1}). The black and blue boxes indicate that the experiment was carried out in the dark or with blue light irradiation.

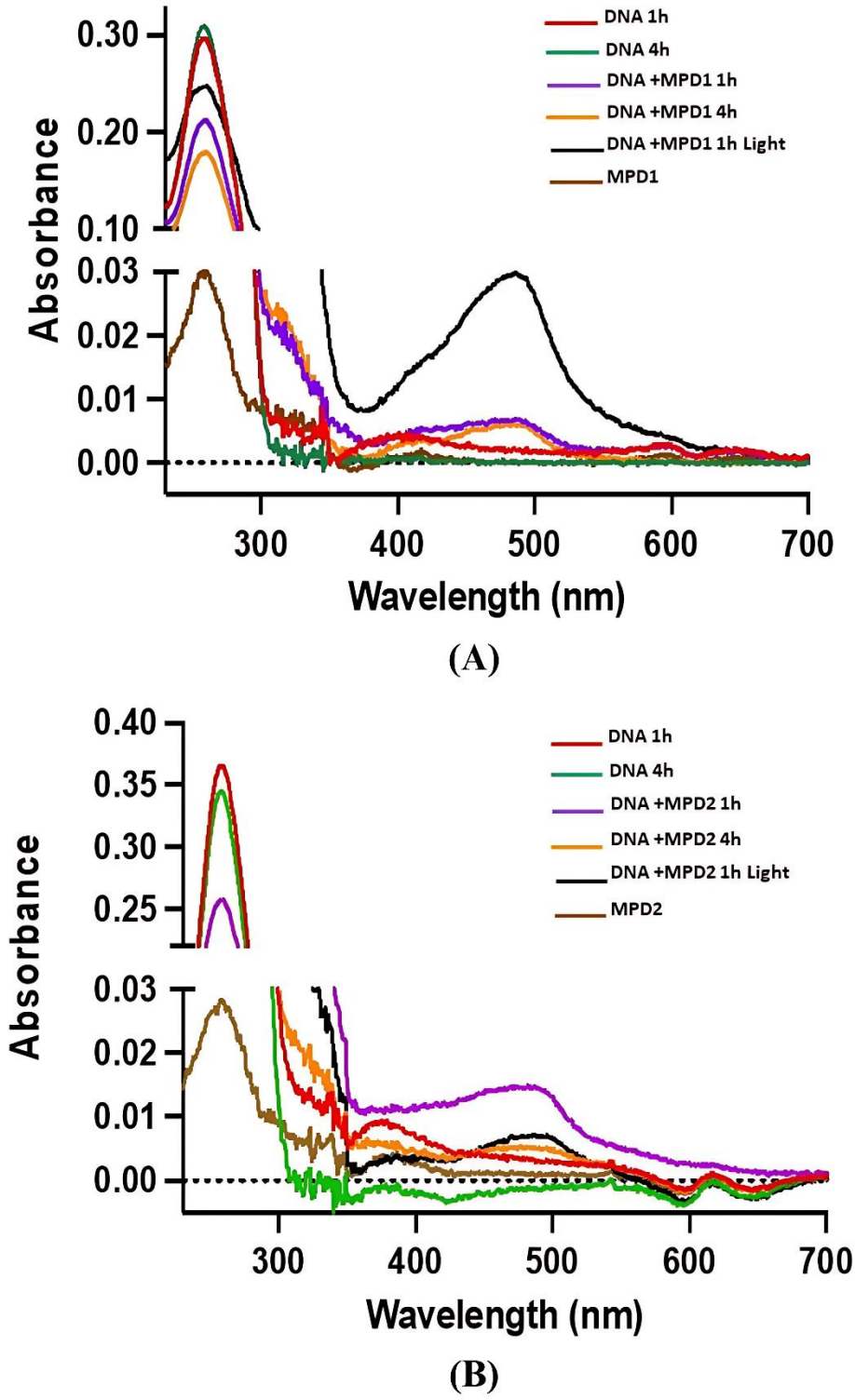

Fig. S17. Electronic spectra for excluded samples upon treatment onto a biospin column P30 (Bio-rad). **MPD1** (A) and **MPD2** (B) (DNA, complex +DNA (dark), complex +DNA (light, $\lambda_{irr.}$=453 nm), DNA, complex).

Table S1. Carbon-13 NMR signal assignment for the MPD1 complex.

^{13}C chemical shifts of the MPD1

Group (Ring A)	δ(ppm)	Ring B	δ(ppm)	Ring C	δ(ppm)	Ring D	δ(ppm)
C5	146,0	C5'	136,83	C5"	137,62	C1	128
C6	120	C6'	124,3	C6"	124,00	C2'	129,5
C7	159,14	C7'	136,83	C7"	137,62	C3	129,7
C8	159,4	C8'	128	C8"	130,6	C4	136,0
C9	120	C9'	153,9	C9"	155		

DFO ligand	δ(ppm)
C2	155
C3	128,8
C4	130,83
C5	130,06
C6	187,7
C7	131,9
C8	132.00
C9	130,94
C10	155,4
C11	167,32
C12	166,13

Table S2. Carbon-13 NMR signal assignment for the MPD2 complex.

^{13}C chemical shifts of the MPD2

Group (Ring A)	δ(ppm)	Ring B	δ(ppm)	Ring C	δ(ppm)	Ring D	δ(ppm)
C5	146	C5'	154,00	C5"	154,00	C1	140,38
C6	124	C6'	124,3	C6"	127,85	C2'	129,5
C7	159,13	C7'	137,55	C7"	137,62	C3	129,56
C8	154	C8'	155	C8"	155,4	C4	134
C9	120	C9'	154,00	C9"	130,6	CH_3	21,5

DFO ligand	δ(ppm)	R-CH_3	δ(ppm)
C2	155	CH_3	21,5
C3	128,8		
C4	137,62		
C5	130,70		
C6	187,95		
C7	131,9		
C8	137,62		
C9	130,98		
C10	155,4		
C11	167,32		
C12	166,13		

Table S3. Selected experimental bands in the FTIR spectrum and the theoretical frequencies, ν(cm^{-1}) of MPD1 and MPD2.

MPD1			**MPD2**		
Experimental	**DFT**	**Assignments**	**Experimental**	**DFT**	**Assignments**
557	516	δ(PF_6)	559	612	δ(PF_6)
850	788	ν(PF_6)	850	788	ν(PF_6)
1580	1516	ν(CN)	1573	1540	ν(CN)
1640	1644	ν(CC)	1608	1628	ν(CC)
1735	1716	ν(CO)	1737	1716	ν(CO)
3044	3196	ν(Csp^2)	2920	3180	ν(Csp^3)
-	-	-	3053	3228	ν(Csp^2)

Table S4. Selected UV−Vis Energy Transitions at the TD-DFT/B3LYP Level for MPD1 in acetonitrile.

Exptl. λ (nm)	**Calc. λ (nm)**	**Major contribution**	**Character**	
510	468	H-1→L+1 (66%)	pπ* (phtpy) ← dπ (Ru)	MLCT
		HOMO→L+3 (28%)	pπ* (phtpy) ← dπ (Ru)	MLCT
		H-2→L+1 (31%)	pπ* (phtpy) ← dπ (Ru)	MLCT
		H-1→L+2(62%)	pπ* (DFO) ← dπ (Ru)	MLCT
		H-1→L+3(94%)	pπ* (phtpy) ← dπ (Ru)	MLCT
364	353	H-3→L+1 (90%)	pπ* (phtpy) ← pπ (phtpy)	IL
		H-4→L+1 (67%)	pπ* (phtpy) ← pπ (phtpy)	IL
		H-3→L+3 (11%)	pπ* (phtpy) ← pπ (phtpy)	IL
314	-	H-3→L+1 (90%)	pπ* (phtpy) ← pπ (phtpy)	IL
		H-4→L+1 (67%)	pπ* (phtpy) ← pπ (phtpy)	IL
283	295	H-7→L+1 (95%)	pπ* (DFO) ← pπ (phtpy)	LLCT
		H-8→L+3 (89%)	pπ* (phtpy) ← pπ (Cl)	LLCT
		H-6→L+3 (30%)	pπ* (phtpy) ← pπ (Cl)	LLCT
		H-4→L+3 (52%)	pπ* (phtpy) ← pπ (phtpy)	IL
231	243	H-4→L+6 (60%)	pπ* (phtpy) ← pπ (phtpy)	IL
		H-10→L+3 (49%)	pπ* (phtpy) ← pπ (phtpy)	IL
		H-4→L+5 (36%)	pπ* (phtpy) ← pπ (phtpy)	IL

Table S5. Selected UV−Vis Energy Transitions at the TD-DFT/B3LYP Level for MPD2 in acetonitrile.

Exptl. λ (nm)	**Calc. λ (nm)**	**Major contribution**	**Character**	
513	470	H-2→L+1 (58%)	pπ* (phtpy) ← dπ (Ru)	MLCT
		H-1→L+2 (35%)	pπ* (DFO) ← dπ (Ru)	MLCT
		H-2→L+2(39%)	pπ* (DFO) ← dπ (Ru)	MLCT
		HOMO→L+3(43%)	pπ* (phtpy) ← dπ (Ru)	MLCT
364	353	H-3→L+1 (95%)	pπ* (phtpy) ← pπ (phtpy)	IL
		H-8→LUMO (95%)	pπ* (DFO) ← pπ (Cl)	LLCT
310	-	H-6→L+1 (20%)	pπ* (phtpy) ← pπ (Cl)	LLCT
		H-4→L+1 (41%)	pπ* (phtpy) ← pπ (phtpy)	IL
		H-3→L+3 (31%)	pπ* (phtpy) ← pπ (phtpy)	IL
276	293	H-6→L+2 (66%)	pπ* (DFO) ← pπ (Cl)	LLCT
		H-5→L+1 (19%)	pπ* (phtpy) ← pπ (phtpy)	IL
		H-6→L+1 (39%)	pπ* (phtpy) ← pπ (Cl)	LLCT
		H-6→L+3 (34%)	pπ* (phtpy) ← pπ (Cl)	LLCT
		H-4→L+3 (53%)	pπ* (phtpy) ← pπ (phtpy)	IL
257	241	H-3→L+7 (74%)	pπ* (phtpy) ← pπ (phtpy)	IL
		H-10→L+3 (43%)	pπ* (phtpy) ← pπ (phtpy)	IL
		H-4→L+5 (42%)	pπ* (phtpy) ← pπ (phtpy)	IL

Table S6. Antimicrobial Assay using **MPD1** and **MPD2**.

Metal Complex	**RED LED**		***P. aeruginosa* ATCC 27854**	***E. coli* ATCC 11303**
MPD1	On	[a]MIC	ND	ND
		[b]MBC	ND	ND
	Off	MIC	ND	ND
		MBC	ND	ND
MPD2	On	MIC	125 (256.48)	125 (256.48)
		MBC	125 (256.48)	ND
	Off	MIC	125 (256.48)	125 (256.48)
		MBC	125 (256.48)	ND
Metal Complex	**BLUE LED**		***P. aeruginosa* ATCC 27854**	***E. coli* ATCC 11303**
MPD1	On	MIC	ND	ND
		MBC	ND	ND
	Off	MIC	ND	ND
		MBC	ND	ND
MPD2	On	MIC	125 (256.48)	125 (256.48)
		MBC	125 (256.48)	ND
	Off	MIC	125 (256.48)	125 (256.48)
		MBC	125 (256.48)	ND

[a]Minimum inhibitory concentration. [b]Minimum bactericidal activity. *MIC and MBC reported in μg/mL (μM). (ND) not detected.